Supplementary Information (SI) for ChemComm.
This journal is © The Royal Society of Chemistry 2026

Supporting Information

Synergistic molecular lock strategy enables efficient and durable wide bandgap perovskite/TOPCon tandem solar cells

Zehang Liu[a], Ruoyu Li[a], Yuzhou Wu[a], Tao Zhang[a], Yaxuan Yang[a], Xinquan Wang[a], Jing Li[a,b], Qingquan He*[a,b], and Jun Pan[a,b]

a. Science and Education Integration College of Energy and Carbon Neutralization, College of Materials Science and Engineering, Zhejiang Provincial Key Laboratory of Clean Energy Conversion and Utilization, State Key Laboratory of Green Chemical Synthesis and Conversion, Zhejiang University of Technology, Hangzhou 310014, P. R. China.

b. Zhejiang Baima Lake Laboratory Co., Ltd., Hangzhou 310000, Zhejiang, P. R. China. Email: qqhe21@zjut.edu.cn

Experimental Section

Materials

Lead iodide (PbI_2, 99.99%), lead bromide ($PbBr_2$, >98%), lead chloride ($PbCl_2$, >99.5%), cesium iodide (CsI, >99%), [4-(3,6-Dimethyl-9H-carbazol-9-yl)butyl]phosphonic Acid (Me-4PACz) were bought from TCI (Shanghai) Development Co., Ltd. Methylammonium chloride (MACl, 99.5%), NiO_x nanoparticle powder (99.999%) and piperazine hydroiodide (PI, 99.5%) were purchased from Xi'an Yuri solar Co., Ltd. 2,2',7,7'-Tetrakis-(N,N-di-4-methoxyphenylamino)-9,9'-spirobifluorene (Spiro-OMeTAD, >99.5%) were supplied by Suzhou LiWei Tech Co., Ltd. Tetraethyl (anthracene-9,10-diylbis(methylene))bis(phosphonate) (EnPO) was bought from Shanghai Bepharm Science&Technology Co., Ltd. Formamidinium iodide (FAI, >99.99%) was obtained from Greatcell Solar Materials. Fullerene (C_{60}, >99.95%) was purchased from Nano-c. All the ultra-dry solvents including anisole (99.7%), N,N-dimethylformamide (DMF, 99.99%), dimethyl sulfoxide (DMSO, 99.99%), isopropanol (IPA, 99.5%), and ethanol (EtOH, 99.8%) were obtained from Sigma Aldrich. All materials were used as received without further purification.

Device Fabrication

Wide-bandgap perovskite solar cells (WBG PSCs).

ITO-coated glass substrates underwent a multi-step cleaning process involving 15 minutes ultrasonic baths in glass detergent, deionized water, ethanol, and IPA, respectively. After a 2 minutes oxygen plasma activation, an aqueous NiO_x nanoparticle dispersion (5 mg mL^{-1}) was spin-coated at 3000 rpm for 30 seconds. The resulting NiO_x films were annealed at 150 °C for 10 minutes in ambient air before being transferred to a nitrogen-purged glovebox. Subsequently, a Me-4PACz self-assembled monolayer

was formed by depositing 90 μL of a 0.5 mg mL^{-1} DMF solution onto the NiO_x surface (3000 rpm, 30 seconds), followed by a 100 °C thermal treatment for 10 minutes.

The WBG perovskite precursor (1.6 mol L^{-1}, $FA_{0.80}MA_{0.15}Cs_{0.05}Pb(I_{0.75}Br_{0.25})_3$) was synthesized by dissolving FAI, MAI, CsI, PbI_2, and $PbBr_2$ in a DMF/DMSO solvent mixture (4:1 v/v). For the experimental groups, the EnPO additive was incorporated into the precursor at varied concentrations (0.3, 0.5, and 0.7 mg mL^{-1}). The films were realized *via* an anti-solvent method: 90 μL of the precursor was spun at 4500 rpm for 40 s with 250 μL of CB quenched at the 20^{th} second. Post-deposition annealing was conducted at 100 ℃ for 20 minutes. A PCBM solution (20 mg mL^{-1} in CB) was then applied as the electron transport layer (2000 rpm, 30 seconds), followed by a brief 1-minute bake at 100 °C. For the buffer layer, a saturated BCP solution in IPA (2 mg mL^{-1} in IPA) was spin-casted at 5000 rpm for 30 s and annealed at 100 °C for 1 minute. Finally, a 100 nm silver (Ag) cathode was thermally evaporated under high vacuum (4×10^{-4} Pa) through a defined shadow mask.

Perovskite/TOPCon tandem solar cells (P/T TSCs).

The fabrication of TOPCon bottom solar cells using Cz phosphorus-doped n-type mono-crystalline silicon wafers was conducted by our collaborator, Chint New Energy Technology (Haining) Co., Ltd. The wafer surface was first textured by traditional industrial alkaline texturing using KOH and organic additive solution. The P^+:Si was formed in a boron diffusion furnace using a BCl_3 source. A thin SiO_x layer is thermally grown on the front side and subsequently cap the interfacial oxide by a low-pressure chemical vapor deposited intrinsic poly-Si layer. The intrinsic poly-Si was doped in a $POCl_3$ diffusion furnace to form n-poly:Si. The rear side is passivated with a stack of aluminum oxide (AlO_x), silicon nitride (SiN_x). Ag paste was screen-printed on the rear

side and fired in a belt furnace to form ohmic contacts. Next, the TOPCon bottom solar cells were laser-cut into 2.5 cm × 2.5 cm substrates for tandem cell fabrication.

The monolithic P/T TSCs were constructed on textured crystalline silicon wafers featuring a TOPCon architecture, utilizing deposition protocols consistent with the single-junction WBG PSCs. Prior to fabrication, the TOPCon silicon substrates received UV irradiation to enhance surface energy and wettability. To ensure uniform coverage over the silicon pyramids and prevent shunting, the perovskite precursor concentration was adjusted to 1.7 mol L^{-1}. Following the perovskite crystallization, a PI passivation layer, a C60 electron transport layer, and an ALD-deposited SnO_2 hole-blocking layer were sequentially integrated. A 40 nm transparent indium zinc oxide (IZO) electrode was then sputtered at 800 W through a 1.1×1.1 cm^2 aperture mask. Metallization involved the thermal evaporation of a 400 nm Ag grid on the perovskite side at 1 Å s^{-1} and a 400 nm Ag full contact on the rear silicon side at 2 Å s^{-1} through a 1.2×1.2 cm^2 aperture mask. The device fabrication was finalized by evaporating a 100 nm LiF anti-reflection coating to optimize light harvesting.

Characterizations

Fourier-transform infrared (FTIR) spectroscopy experiments were carried out on Thermo Fisher Scientific Nicolet iS50. ^1H nuclear magnetic resonance spectroscopy (NMR) spectra were collected on a Bruker 400 MHz spectrometer and referenced to the residual solvent peaks of *DMSO-d6* at 2.50 and 39.50 ppm, respectively. X-ray photoelectron spectroscopy (XPS, Thermo Scientific K-Alpha) was performed using Al-Kα radiation (1486.6 eV) to analyze elemental chemical states. X-ray diffraction (XRD) patterns were obtained with a Cu-Kα source (λ = 0.154187 nm). Surface

morphology was examined by scanning electron microscopy (SEM, Nova NanoSEM450) and atomic force microscopy (AFM, Bruker Dimension). Contact angles were measured with an optical goniometer (OAC30, JMH Technology) by depositing ultrapure water droplets on film surfaces.

Steady-state photoluminescence (PL) spectra were measured using a Horiba Quanta Master 8000 instrument. The 2D PL mapping was executed by Full-Field Scanning (QFLS-Maper). Time-resolved PL (TRPL) measurements were carried out using an FLS1000 system from Edinburgh Instruments, with an excitation wavelength of 445 nm. Electronic structure and optical properties were assessed *via* ultraviolet photoelectron spectroscopy (UPS, Thermo Fisher EscaLab 250Xi). Electrochemical impedance spectroscopy (EIS) was conducted on a Zahner Zennium workstation over a frequency range of 1 MHz to 0.1 Hz. The current-density-voltage (*J-V*) characteristics of solar cells were measured using Keithley 2400 source meter under the illumination of a solar simulator (Japan, SAN-EI, XES-40S1). For single-junction WBG PSCs, an optical mask with an aperture area of 0.09 cm^2 was employed, while the P/T TSCs were measured using a mask with an opening of 1.004 cm^2. The EQE spectrum was measured using QE-RX (Enlitech Co., Ltd.). The light intensity at each wavelength was standardized utilizing a reference single crystal silicon photovoltaic cell. The stability of the device was evaluated under AM 1.5G illumination at a light intensity of 100 mW cm^{-2} across various conditions. The dark current density was assessed using a semiconductor parameter analyzer (Keithley 2400).

Space charge limited current measurement (SCLC)

SCLC was assessed through current-voltage scanning of hole-only devices constructed with a glass/ITO/HTL/Perovskite/Spiro-OMeTAD/Au configuration. The spiro-

OMeTAD hole-transporting layer was deposited by spin coating a precursor solution consisting of 72.3 mg spiro-MeOTAD, 28.8 μL 4-tert-butylpyridine, 17.5 μL Li-TFSI solution (520 mg ml^{-1} in acetonitrile) in 1 ml chlorobenzene onto the perovskite layer. The current-voltage scan measurement was carried out by Keithley 2400 source meter. The trap density (N_{trap}) can be calculated using the following equation:

$$N_{trap} = \frac{eV_{TFL}L^2}{2\varepsilon\varepsilon_0} \quad (1)$$

where e, ε, ε_0 *and* L represent the elementary charge, the relative permittivity of the perovskite, the vacuum permittivity, and the thickness of the perovskite film, respectively.

And the hole mobility (μ_h) was obtained by fitting the results to Mott Gurney law for space charge limited current (SCLC) as the following equation:

$$J = \frac{9\varepsilon\varepsilon_0\mu_h V^2}{8L^3} \quad (2)$$

where J is the current density.

Light intensity-dependent V_{OC} analysis

$$V_{OC} = \frac{nk_BT}{q}\ln(I) + B \quad (3)$$

where k_B, *T, q, I, B* represent Boltzmann constant, thermodynamic temperature, the electron charge, light intensity and constant, respectively. The smaller n is theoretically, the indirect defect recombination at the interface (SRH recombination, Shockley-Read-Hall recombination) is smaller.

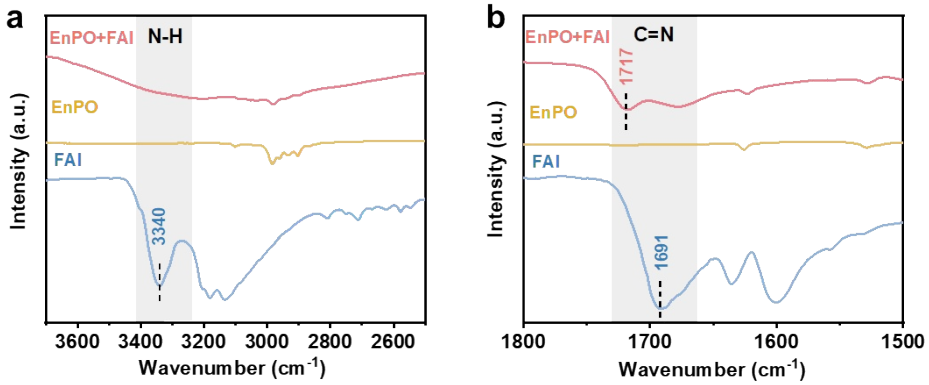

Fig. S1 FTIR spectra of the (a) N-H and (b) C=N stretching vibration regions for FAI, EnPO, and their respective mixtures.

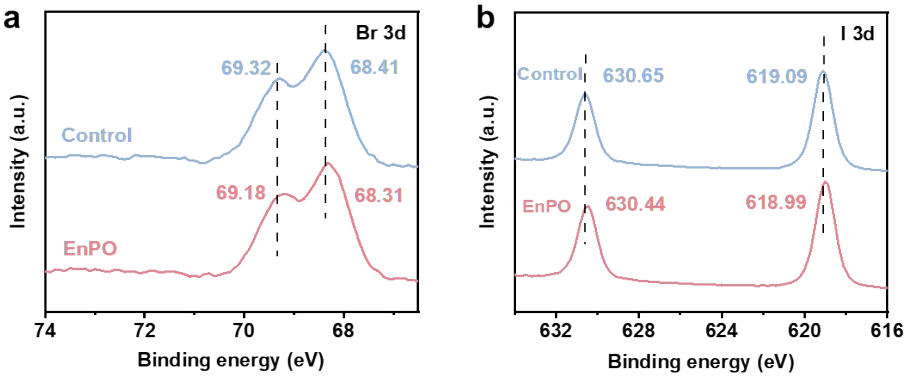

Fig. S2 XPS spectra of (a) Br 3d and (b) I 3d core levels for the control and EnPO-modified perovskite films.

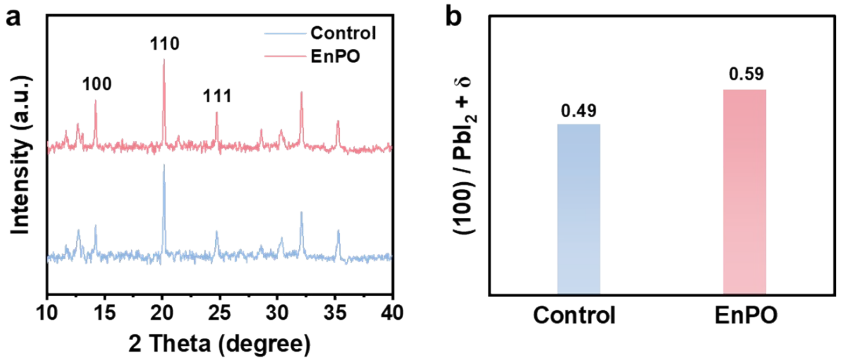

Fig. S3 (a) XRD patterns and the corresponding (100)/(PbI_2+δ) integrated area ratio of the control and EnPO-modified perovskite films.

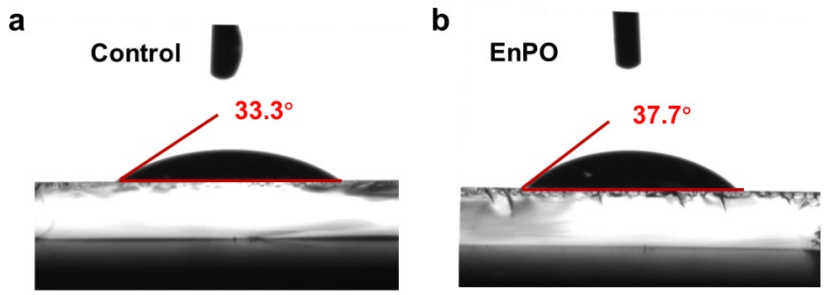

Fig. S4 Water contact angle measurement of the (a) control and (b) EnPO-modified perovskite films.

Table S1. Fitting parameters of TRPL spectra of control and EnPO-modified ITO/NiO_x/Me-4PACz/perovskite devices

Sample	A_1 (%)	τ_1 (ns)	A_2 (%)	τ_2 (ns)	τ_{ave} (ns)[a]
Control	40	3.8	60	2623.7	2621.7
EnPO	40	2.9	60	1524.1	1522.3

[a] Equation 1. $\tau_{ave} = (A_1\tau_1^2 + A_2\tau_2^2) / (A_1\tau_1 + A_2\tau_2)$

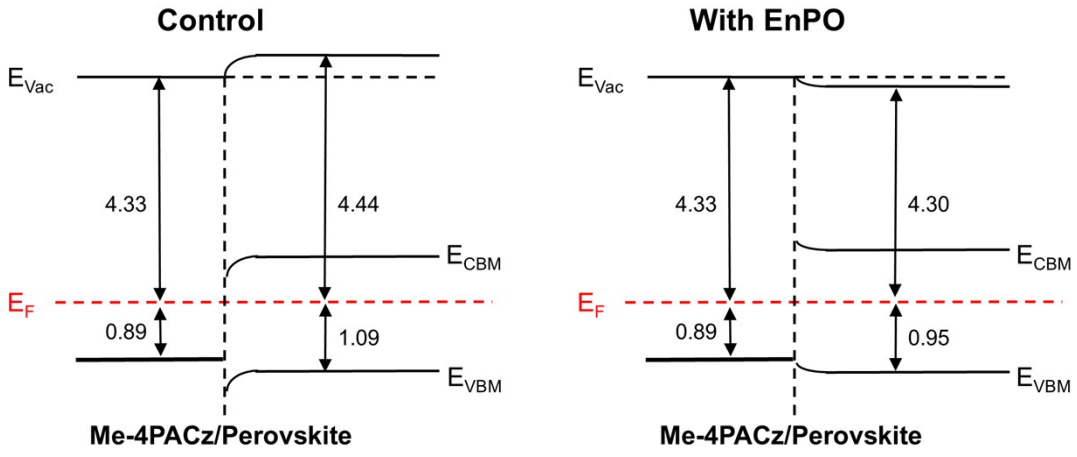

Fig. S5 Schematic illustration of energy-level and band bending in perovskite films with and without EnPO modification.

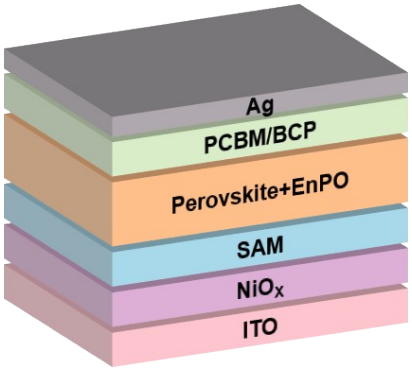

Fig. S6 The device configuration of the 1.68 eV WBG PSCs.

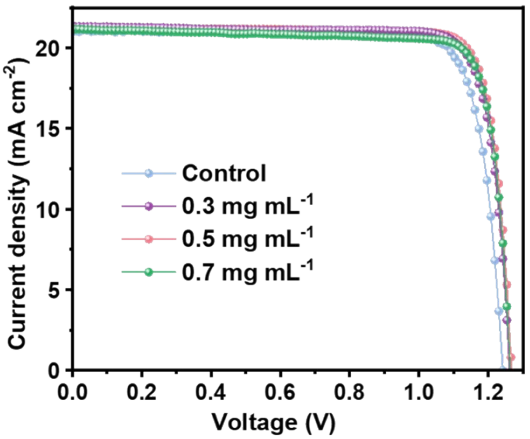

Fig. S7 *J-V* curves of WBG PSCs modified with different concentrations of EnPO.

Table S2. Photovoltaic parameters of WBG PSCs modified with different concentrations of EnPO

Samples	V_{OC} (V)	J_{SC} (mA cm^{-2})	FF (%)	PCE (%)
Control	1.242	21.03	83.26	21.75
0.3 mg mL^{-1}	1.261	21.32	83.51	22.45
0.5 mg mL^{-1}	1.267	21.34	85.06	23.01
0.7 mg mL^{-1}	1.262	21.15	83.92	22.41

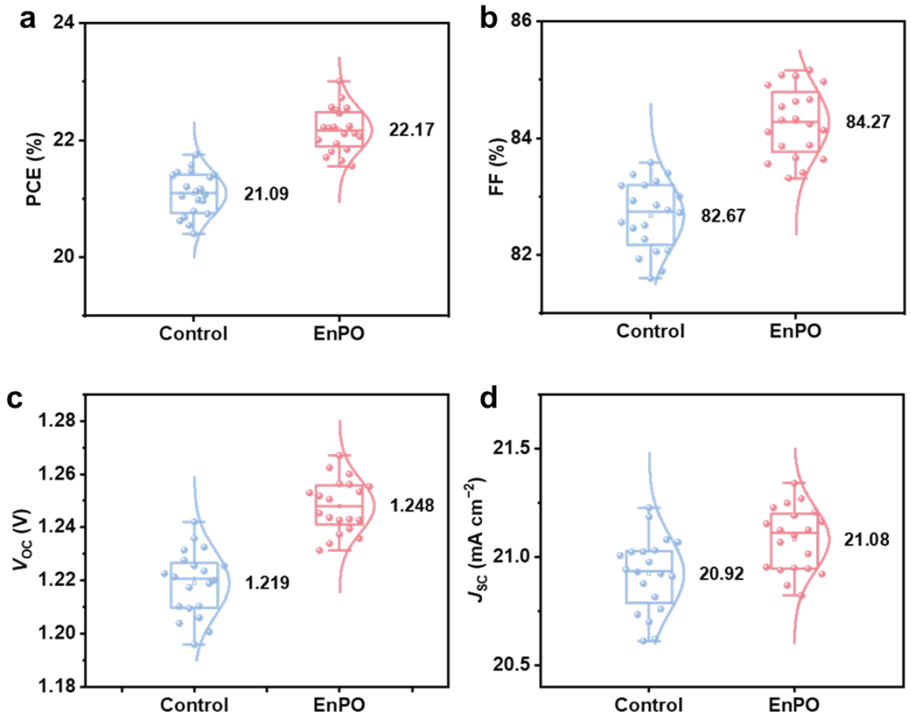

Fig. S8 Distribution statistics of (a) PCE, (b) FF, (c) V_{OC}, and (d) J_{SC} for the control and EnPO-modified WBG PSCs.

Table S3. Photovoltaic parameters of WBG PSCs with and without EnPO modification

Samples	V_{OC} (V)	J_{SC} (mA cm^{-2})	FF (%)	PCE (%)
Control	1.219 ± 0.012	20.92 ± 0.17	82.67 ± 0.59	21.09 ± 0.37
EnPO	1.248 ± 0.010	21.08 ± 0.15	84.27 ± 0.59	22.17 ± 0.37

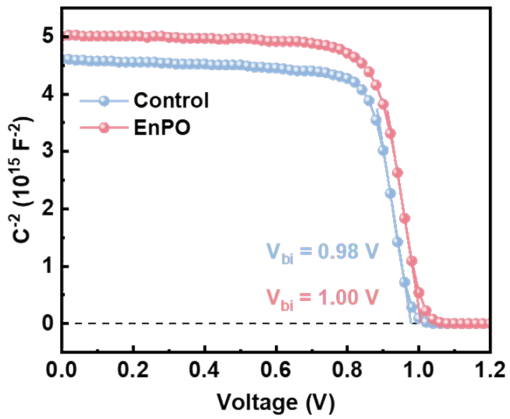

Fig. S9 Mot-Schottky analysis of PSCs with and without EnPO modification.

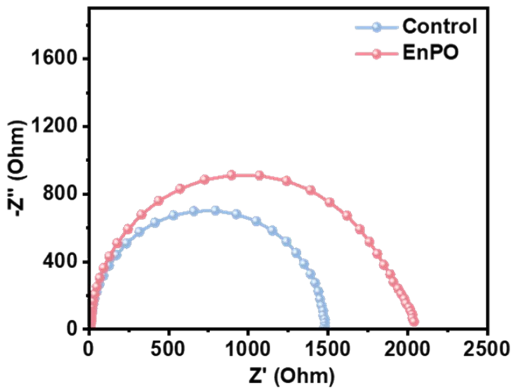

Fig. S10 Nyquist plots of the control and EnPO-modified WBG PSCs measured under dark conditions.

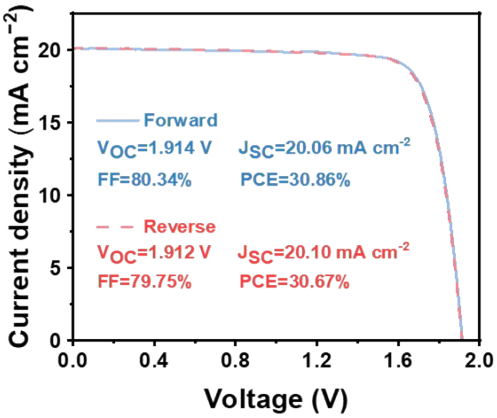

Fig. S11 *J-V* curves of the best-performing control WBG PSCs.

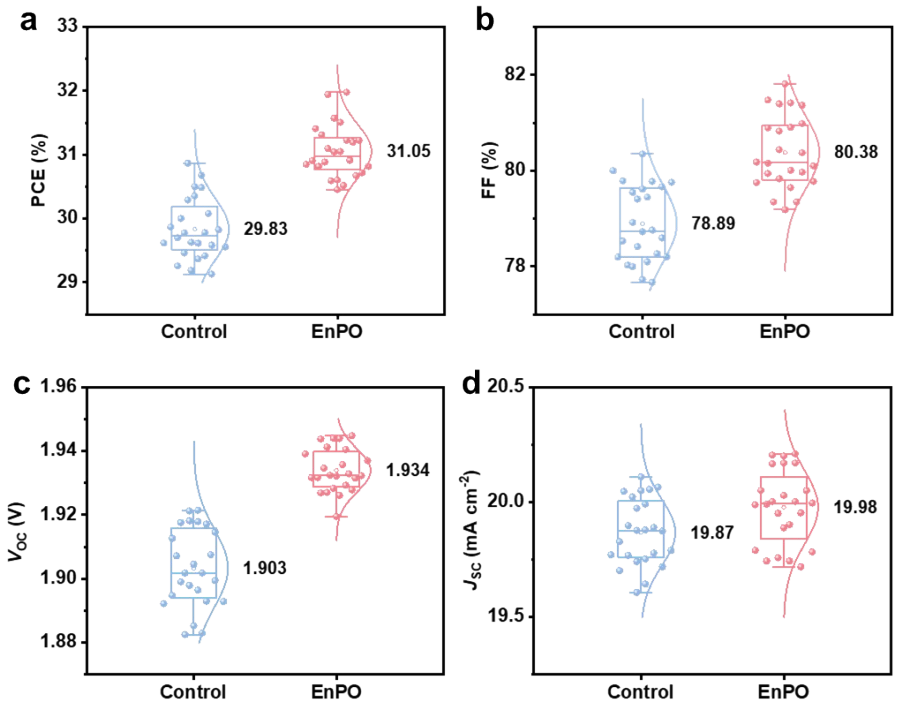

Fig. S12. Distribution statistics of (a) PCE, (b) FF, (c) V_{OC}, and (d) J_{SC} for the control and EnPO-modified P/T TSCs.

Table S4. A Summary of photovoltaic parameters of perovskite/TOPCon tandem solar cells in previous reports

Year	V_{OC} (V)	J_{SC} (mA cm^{-2})	FF (%)	PCE (%)	Reference
2025	1.93	19.89	81.54	31.32	1
2025	1.88	20.0	82.60	31.10	2
2025	2.02	19.76	82.86	33.12	3
2026	1.94	20.20	81.36	31.97	This work
2026	1.95	20.55	83.78	33.62	4

To benchmark our results against recent advancements, the photovoltaic parameters of state-of-the-art perovskite/TOPCon TSCs are summarized in Table S4. While the champion PCE of 31.97% is slightly below the current world records, this work emphasizes a distinct material-centric innovation. By implementing the EnPO-based "molecular lock" strategy, we achieved a superior balance between high efficiency and

exceptional lattice stability. Notably, the high V_{OC} of 1.944 V and the demonstrated thermal resilience, retaining 92% efficiency after 800 h at 65 °C, underscore the efficacy of our dual-site passivation mechanism. This approach provides a robust, generalizable design paradigm for molecular additives that simultaneously regulates crystallization and fortifies the perovskite framework, offering significant value for the commercialization of stable, high-performance tandem photovoltaics.

References

1. L. Wang, N. Wang, X. Wu, B. Liu, Q. Liu, B. Li, D. Zhang, N. Kalasariya, Y. Zhang, X. Yan, J. Wang, P. Zheng, J. Yang, H. Jin, C. Wang, L. Qian, B. Yang, Y. Wang, X. Cheng, T. Song, M. Stolterfoht, X. C. Zeng, X. Zhang, M. Xu, Y. Bai, F. Xu, C. Zhou and Z. Zhu, Advanced Materials, 2025, 37, 2416150.
2. Y. Luo, Y. Tian, K. Zhao, W. Mao, C. Liu, J. Shen, Z. Cheng, C. Değer, X. Miao, Z. Zhang, X. Sun, L. Yao, X. Zhang, P. Shi, D. Jin, J. Deng, M. Tian, I. Yavuz, N. Dong, R. Liu, R. Wang, D. Yang and J. Xue, Nature Communications, 2025, 16, 4516.
3. L. Wang, N. Wang, N. Kalasariya, X. Sun, X. Wu, Z. Yu, B. Li, Y. Qiao, K. Long Wong, A. F. Castro Mendez, O. Karalis, C. Zhang, D. Gao, H. Hempel, J. Wang, J. Yang, H. Jin, Y. Bai, X. Zhang, M. Xu, T. Unold, F. Lang, J. Yin, M. Stolterfoht and Z. Zhu, Joule, 2025, 9, 102174.
4. Q. Zhou, R. Guo, S. Liu, N. Li, M. Xu, X. Zhang, X. Jiang, L. Wang, L.-I. Dion-Bertrand, Z. Shi, X. Guo, H. Liang, Z. Dong, J. Chen, Y.-D. Wang, R. Luo, X. Wang, J. Wang, J. Yang, H. Jin, C.-H. Kuan, S.-F. Hung, Z. Jia, L. K. Lee, D. Lai, E. W.-G. Diau, W. Yan and Y. Hou, Nature Energy, 2026, https://doi.org/10.1038/s41560-026-02010-z.